PNAS RESEARCH ARTICLE | CELL BIOLOGY

PRD-2 mediates clock-regulated perinuclear localization of clock gene RNAs within the circadian cycle of *Neurospora*

Bradley M. Bartholomai[a], Amy S. Gladfelter[b], Jennifer J. Loros[c], and Jay C. Dunlap[a,1]

Edited by Joseph Takahashi, The University of Texas Southwestern Medical Center, Dallas, TX; received February 20, 2022; accepted June 24, 2022

The transcription–translation negative feedback loops underlying animal and fungal circadian clocks are remarkably similar in their molecular regulatory architecture and, although much is understood about their central mechanism, little is known about the spatiotemporal dynamics of the gene products involved. A common feature of these circadian oscillators is a significant temporal delay between rhythmic accumulation of clock messenger RNAs (mRNAs) encoding negative arm proteins, for example, *frq* in *Neurospora* and *Per1-3* in mammals, and the appearance of the clock protein complexes assembled from the proteins they encode. Here, we report use of single-molecule RNA fluorescence in situ hybridization (smFISH) to show that the fraction of nuclei actively transcribing the clock gene *frq* changes in a circadian manner, and that these mRNAs cycle in abundance with fewer than five transcripts per nucleus at any time. Spatial point patterning statistics reveal that *frq* is spatially clustered near nuclei in a time of day–dependent manner and that clustering requires an RNA-binding protein, PRD-2 (PERIOD-2), recently shown also to bind to mRNA encoding another core clock component, casein kinase 1. An intrinsically disordered protein, PRD-2 displays behavior in vivo and in vitro consistent with participation in biomolecular condensates. These data are consistent with a role for phase-separating RNA-binding proteins in spatiotemporally organizing clock mRNAs to facilitate local translation and assembly of clock protein complexes.

Neurospora | circadian rhythms | cell biology | smFISH | liquid–liquid phase separation

Significance

Circadian clocks are molecular feedback loops that operate similarly in animals and fungi. While we know much about genes and proteins that comprise a clock, we know very little about where in the cell clocks are assembled and operate. By following the locations of single messenger RNA (mRNA) molecules in snapshots of cells across time, we see that mRNAs encoding a core clock protein, FRQ, are clustered near nuclei, a result of their interaction with the RNA-binding protein PRD-2, which also binds other RNAs. Disruption of this RNA-binding interaction by eliminating PRD-2 results in a long circadian period. These data are consistent with a model where RNAs encoding clock proteins are organized and sequestered within cells, contributing to posttranscriptional regulation.

Circadian rhythms have been observed throughout all kingdoms of life. The core mechanisms of the molecular timekeepers that give rise to physiological outputs of circadian phenotypes have been meticulously studied and solved in several model systems (1–5). In recent years, an interest in understanding the spatiotemporal dynamics of molecular clocks at the cellular level has emerged (6,7). The majority of early cell biology work surrounding the clock focused on whether the core clock molecules were localized in nuclei or the cytoplasm and at what time of day translocations occur (8, 9). Advancements in our understanding of cytoplasmic and nuclear organization have revealed that such a simplistic binary understanding of localization is insufficient to understand how trafficking of clock molecules might contribute to the time delays that are intrinsic to the overall mechanism of these highly regulated biochemical processes (10–12).

The fundamental regulatory mechanisms of all animal and fungal clocks are remarkably similar albeit with varying levels of complexity. At the root of these clocks is a phosphorylation-driven transcription–translation negative feedback loop (13, 14) in which heterodimeric transcription factors drive expression of genes encoding proteins that form complexes which depress the activity of the transcription factor heterodimers. The most simple and well-studied of these is the molecular clock in the filamentous fungus *Neurospora crassa*. The key players in *Neurospora*'s clock are FREQUENCY (FRQ), FRQ-interacting RNA helicase (FRH), and casein kinase-1a (CK-1a) in the negative arm, and the heterodimeric transcription factor composed of WHITE COLLAR-1 (WC-1) and WHITE COLLAR-2 (WC-2) known as the WHITE COLLAR complex (WCC) in the positive arm. Late at night, the WCC initiates expression of *frq*. The intrinsically disordered FRQ protein (15, 16) forms a homodimer and is stabilized in a complex with FRH and CK-1a known as the FRQ–FRH complex (FFC). FRQ is progressively phosphorylated at over 100 known phosphorylation sites in a carefully orchestrated manner over an ∼22-h period (17, 18), a process facilitated by CK-1a. At some point the FFC enters the nucleus and interacts with the WCC. This interaction leads to phosphorylation of the WCC, which destabilizes its interaction with DNA, effectively repressing the transcription of *frq* and other clock-controlled genes (19). Upon reaching a state of maximum phosphorylation, the heteromultimeric clock complex dissociates, releasing the WCC; FRQ is later targeted to the proteosome for degradation, although

Author affiliations: [a]Department of Molecular and Systems Biology, Geisel School of Medicine at Dartmouth, Hanover, NH 03755; [b]Department of Biology, University of North Carolina at Chapel Hill, Chapel Hill, NC 27599; and [c]Department of Biochemistry and Cell Biology, Geisel School of Medicine at Dartmouth, Hanover, NH 03755

Author contributions: B.M.B., A.S.G., J.J.L., and J.C.D. designed research; B.M.B. performed research; B.M.B., A.S.G., J.J.L., and J.C.D. contributed new reagents/analytic tools; B.M.B. and J.C.D. analyzed data; B.M.B. and J.C.D. wrote the paper; and A.S.G. and J.J.L. edited the paper.

The authors declare no competing interest.

This article is a PNAS Direct Submission.

[1]To whom correspondence may be addressed. Email: jay.c.dunlap@dartmouth.edu.

This article contains supporting information online at http://www.pnas.org/lookup/suppl/doi:10.1073/pnas.2203078119/-/DCSupplemental.

Published July 26, 2022.

the timing of this appears not to be important for period determination (20). Active WCC arises from de novo synthesis or from dephosphorylation and is free to drive renewed expression of *frq*, beginning the cycle once again. Although much is known about the genetic and biomolecular underpinnings of this process, little is known about the intracellular trafficking of the molecules involved within *Neurospora*'s complex syncytial network of hyphae.

An interesting phenomenon has been observed in which the peak of *frq* messenger RNA (mRNA) accumulation occurs several hours before the peak of FRQ protein accumulation (21, 22), and 6 to 8 h are typically required from the time the WCC begins to express *frq* to the point at which clock protein complexes are assembled and can repress further *frq* expression. Given the half-life of about 15 min for *frq* transcripts (23, 24), we became curious as to what mechanisms might be at play that either stall *frq* translation or protect a small subset of *frq* transcripts so enough copies are present when it is time for translation to occur. This phenomenon is not unique to *frq*, or to *Neurospora*. For instance, in recent studies, we found that among a subset of genes that were rhythmic at both the mRNA and protein level, over 80% had a delay of at least 2 h between peak mRNA accumulation and peak protein accumulation, with a mean delay of 10.3 h (22, 25). Similar multihour delays are also seen between the peaks of *Per1/Per2* mRNA and Per1/Per2 in the mouse (26). Because posttranscriptional and potentially posttranslational regulation can involve RNA-binding proteins, our interest was sparked by the finding that the recently cloned *Neurospora* RNA-binding protein encoded by the clock gene *prd-2* interacts with *ck-1a* mRNA and thereby influences period length of *Neurospora*'s overt circadian rhythm. Knockout strains of PRD-2 have a period length about 3 h longer than wild type (23).

To begin investigation of the delays between RNA and protein expression peaks for core clock components, and to understand how *frq* transcripts are localized in *Neurospora* hyphae, we adapted single-molecule RNA fluorescence in situ hybridization (smFISH) for use in *Neurospora* (27), revealing that *frq* transcripts are nonrandomly clustered with nuclei when expressed during the circadian cycle. Surprisingly, despite robust cycling of *frq* transcript levels, only a small subset of nuclei are actively transcribing *frq* at any given time as it cycles in abundance throughout the circadian day. The nonrandom clustering of *frq* near nuclei is mediated by the PRD-2 RNA-binding protein and there is a direct interaction between *frq* mRNA and PRD-2. PRD-2 is an intrinsically disordered protein (IDP) that forms ordered gel-like assemblies in vitro and micrometer-scale assemblies in vivo that are deformable and fuse. These data led to a model in which assemblies of PRD-2, protein, with *frq*, and *ck-1a* mRNAs form to posttranscriptionally regulate the clock in time and space.

Results

***frequency* mRNA Can Be Detected and Quantified Using Single-Molecule RNA FISH.** smFISH was recently adapted for use in *Neurospora* (27–29). Forty-eight fluorescently labeled oligonucleotides designed to bind the protein-coding sequence of *frequency* mRNA enable resolution of individual transcripts (Fig. 1*A*). smFISH puncta were not observed in a *Δfrq* strain when hybridized with *frq* smFISH probes, but were observed in the same strain when hybridized with probes designed to target the G1/S cyclin *cln-1* (Fig. 1*B*). The density of *cln-1* mRNA appears similar to what has been previously observed in its *Ashbya gossypii* ortholog (29). Individual transcripts are identified as those smFISH puncta that fall within 15% of the histogram peak for integrated density values, normalized by *z* score. Puncta that do not meet the criteria for individual transcripts are considered as noise or as multiple transcripts in the same location if they fall below or above the threshold, respectively (Fig. 1*C*). *frq* mRNA is both clock-regulated as a part of its function in the oscillator and light-induced as a part of circadian entrainment (30, 31), so the following conditions were used to benchmark expression levels as visualized by smFISH. *Neurospora* hyphae from dispersed liquid cultures were subjected to analysis. Given the nature of the dispersed culture, fixation, and extensive processing, images were collected from all regions of the apparently healthy growing cells, irrespective of their proximity to an apical tip or vestigial conidial body. In constant light (LL), hyphae were found to have approximately three *frq* transcripts per nucleus. At the first mRNA accumulation peak in constant dark free running conditions (DD16/CT5; DD, time in hours free running in constant darkness; CT, circadian time), approximately two *frq* transcripts were observed per nucleus (Fig. 1*D*). These controls and primary observations provided confidence that this technique could be used to robustly probe spatiotemporal patterning and localization of *frequency* mRNA throughout the circadian cycle.

Transcription of *frequency* Is Spatially Heterogeneous and Transcripts Cycle in Abundance throughout the Day. Previous studies using bioluminescence or traditional biochemical methods have established a robust rhythm of *frq* accumulation and degradation over a period of multiple days in free running conditions (21, 30, 32). To investigate how robust and synchronous this pattern of expression is at the cellular level, smFISH was performed on *Neurospora* hyphae collected at an interval of 4 h for 36 h using established methods (22, 27, 33). To ensure the comparison of hyphae with similar cellular compositions, the ratio of nuclei to volume was measured for all sets of hyphal images and analyzed (*SI Appendix*, Fig. S1*A*). These data indicate that there are not significant differences in cellular composition among images analyzed for this work using this metric. Accepting these controls, a clear pattern of *frq* smFISH puncta is observed over time in hyphal segments (Fig. 2*A*).

There are many factors that influence the timing of transcription and nuclear export in eukaryotes, and smFISH is limited in what it can tell us surrounding transcriptional activity. However, we reason that transcripts that are fully colocalized within nuclei have not yet been exported and indicate recent transcription on an order of tens of minutes based on estimations from various eukaryotic transcription and export rate analyses (34–37) and the ∼5-kb size of the *frq* transcript. To approximate how transcriptional activity of *frq* changes throughout the day, colocalization between *frq* mRNA and nuclei was quantified using a stringent metric of 100% three-dimensional (3D) pixel overlap of mRNA puncta with nuclear signal from *z* stacks, using object-based colocalization (Fig. 2*B*). Transcriptional hotspots have been shown to be brighter than individual transcripts, indicating the presence of multiple nascent or newly completed transcripts in the same location (28). Therefore, only foci with integrated density values greater than or equal to those of individual transcripts were used in this analysis. Transcriptional activity was highest in the late subjective night and early subjective morning (CT22 to CT5), but even at these times only about a third of nuclei were seen to contain *frq* transcripts. In the subjective evening and night (CT14 to CT21), transcriptional activity was lowest, with many hyphal segments not containing any nuclei that are producing *frq* (Fig. 2*C*). The circadian pattern observed in this approximation of transcriptional activity is consistent with

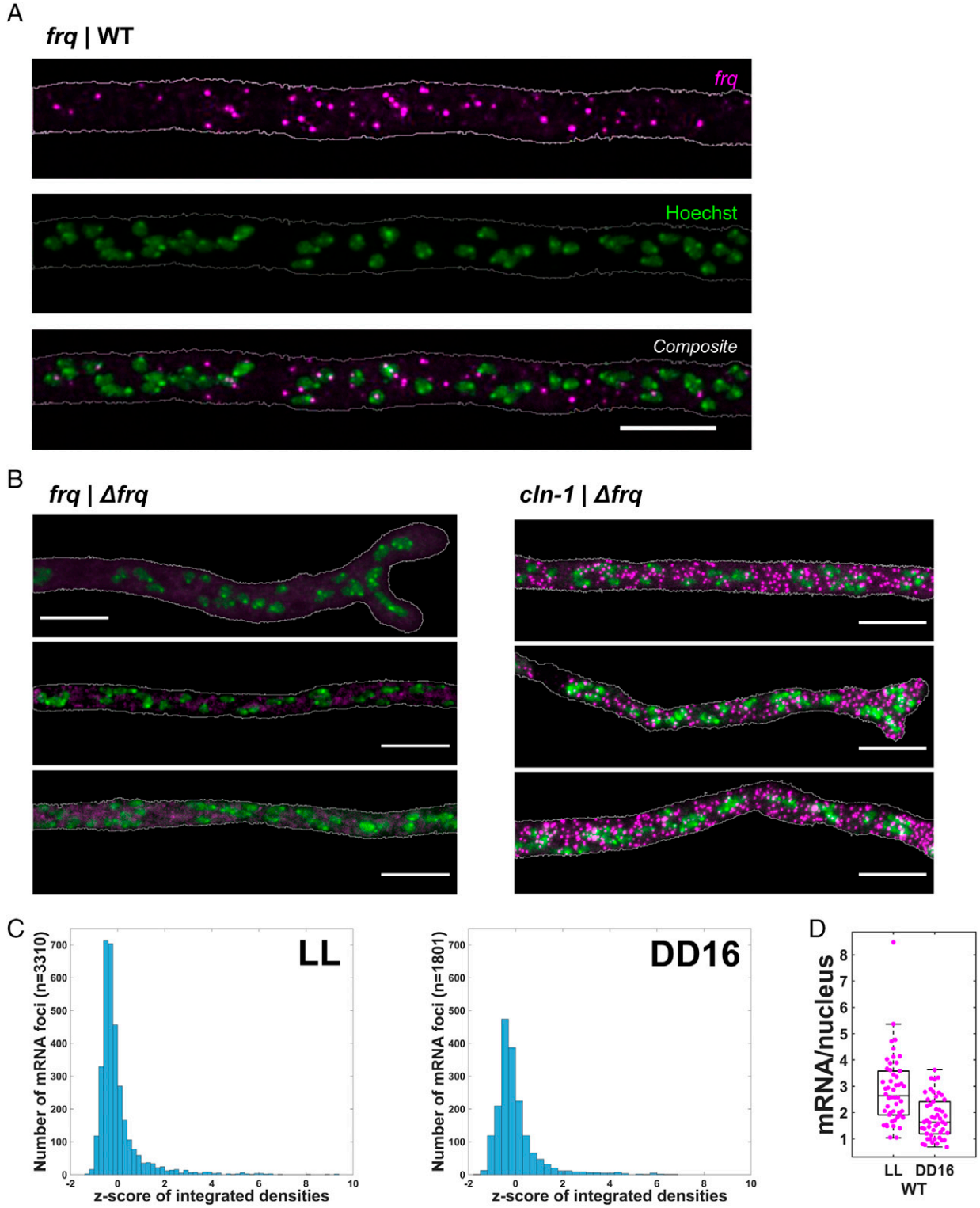

Fig. 1. *frequency* transcripts can be detected and quantified using smFISH. (*A*) Wild-type (WT) *N. crassa* hybridized with *frq* mRNA–specific Quasar 647–conjugated oligonucleotides (magenta) and Hoechst 33342–stained nuclei (green) shown as individual channels and a composite of both channels. (*B*) Composite smFISH images of *frq*-specific and *cln-1*–specific Quasar 647–conjugated oligonucleotides (magenta) and Hoechst 33342–stained nuclei (green) in a *Δfrq* mutant strain of *N. crassa*. (*C*) Histograms of integrated density values for detected *frq* mRNA foci in 50 images from four biological replicates for both constant light and the first circadian mRNA peak in free running conditions (DD16/CT5), both used to quantify individual transcripts. (*D*) Boxplots representing the ratio of *frq* mRNA to nuclei and volume in LL and DD16. Hyphal boundaries are indicated by gray outlines. (Scale bars, 10 μm.)

rhythms observed by a bioluminescent clock reporter in which the *frq* promoter drives expression of firefly luciferase (32).

Quantification of the ratio of *frq* transcripts to nuclei shows rhythmic expression with peaks early in the subjective day and troughs in the subjective night at times and with amplitudes consistent with previous observations (21, 22, 30). Prior estimates were, however, derived from cell extracts where heterogeneity among nuclei could not be observed. Here it is plain that there is a great deal of variability among nuclei, although there are relatively small changes in the absolute number of *frq*

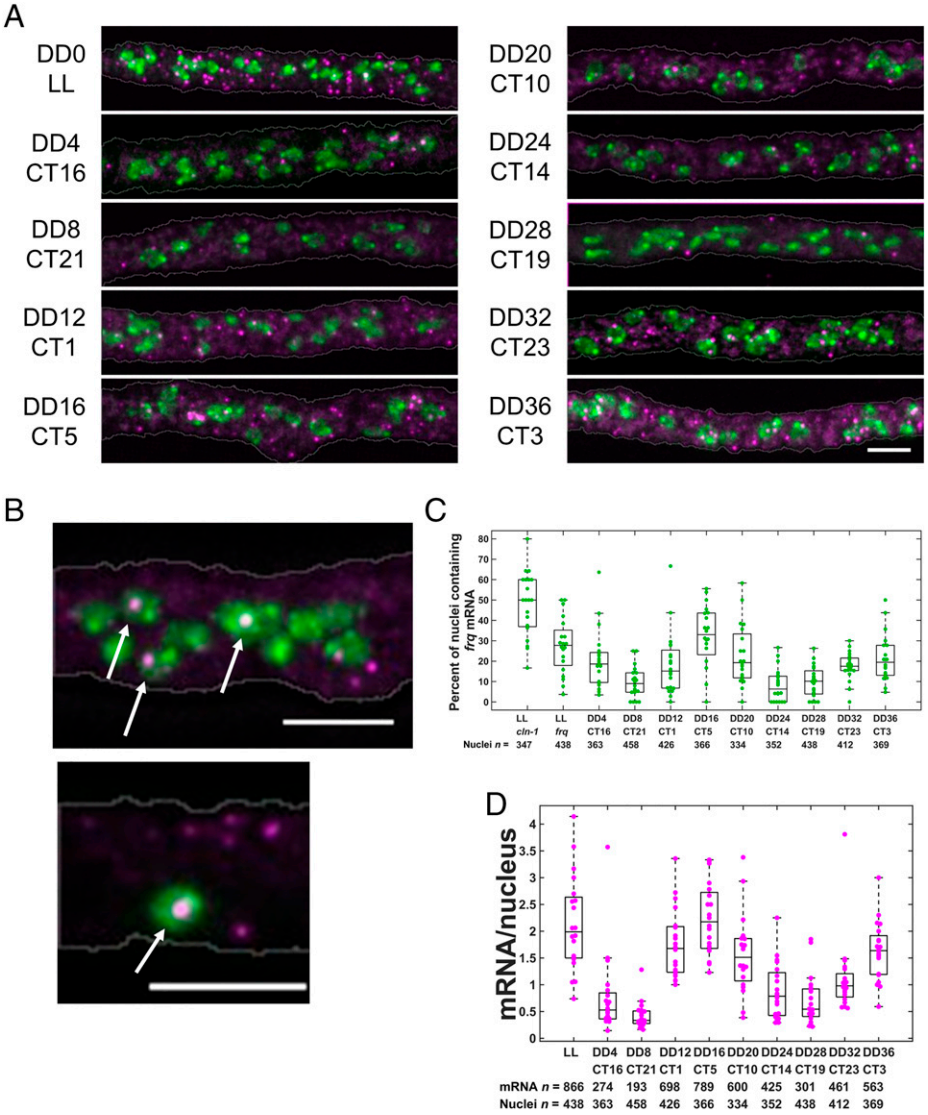

Fig. 2. *frequency* mRNA cycles in abundance throughout the day. (*A*) Composite images of *frq* mRNA (magenta) and nuclei (green) in wild-type free running (constant darkness) *N. crassa* sampled every 4 h for 36 h. (Scale bar, 5 μm.) (*B*) Composite images of *frq* mRNA (magenta) and nuclei (green) shown as maximum-intensity *Z* projections. Arrows indicate nuclei containing colocalized *frq* transcripts. Hyphal boundaries are indicated by gray outlines. (Scale bars, 5 μm.) (*C*) Boxplot approximating the percentage of nuclei actively transcribing *frq* as determined by the number of nuclei containing colocalized *frq* transcripts. (*D*) Boxplot comparing the ratio of *frq* mRNA to nuclei in multiple images ($n = 20$) at each time point in a free running circadian experiment.

transcripts present throughout the day (Fig. 2*D*). Multiple-comparison analysis using Tukey's HSD (honestly significant difference) revealed statistical similarity in transcript abundance from subjective dawn to subjective dusk and from subjective dusk to subjective dawn, and statistically significant differences between the two groups (subjective day vs. night) (*SI Appendix*, Fig. S1*B*). In hyphal segments, as many as 6 *frq* transcripts per nucleus are observed in the early subjective morning (DD16/CT5) and as few as 0 in the subjective night (DD28/CT19), so although the average only oscillates between about 1 and 2.5 transcripts per nucleus, there are almost always nuclei that appear transcriptionally quiescent in terms of core clock gene expression.

***frq* Is Nonrandomly Positioned in the Cytoplasm and Clusters with Nuclei.** Our initial examination of the data from Figs. 1 and 2 suggested that mRNAs were not homogeneously dispersed within the hyphal cytoplasm so, to evaluate mRNA patterning, we applied spatial point patterning statistics using Ripley's K (38, 39). The center of mass was determined for all nuclei, which are about 1 to 2 μm in diameter (40). *X*, *Y*, and *Z* distances between nuclei and mRNAs were then determined for all mRNA puncta and nuclei in each hyphal segment using Fiji and arivis Vision4D as conceptualized in Fig. 3*A*. The Ripley's K determination was performed for each of the mRNA puncta and plotted as described by Lee and colleagues (28, 29). To generate 95% CIs for RNA locations corresponding to a random distribution, the measured number of mRNA puncta was randomly placed in a spherical region of interest surrounding nuclei, which was iterated 100 times. The aggregated data were normalized to the upper bounds of the 95% CI. Finally, a median clustering index was used to identify distances from any given nuclear center of mass where nonrandom clustering is observed ($\gamma > 1$) (Fig. 3 *A*, *vii*).

In constant light, *frq* is broadly, but clearly nonrandomly, clustered in relationship to nuclei. As an internal control for random clustering, the housekeeping gene *ad-18* (NCU16511) was chosen because it is constitutively expressed at a similar level to *frq* (22, 23, 27) and was not predicted to have any specialized localization reflecting its ubiquitous role in nucleotide biogenesis. Specific probes for *ad-18* were hybridized to wild-type *N. crassa*, imaged, and analyzed. The mean value of *ad-18*

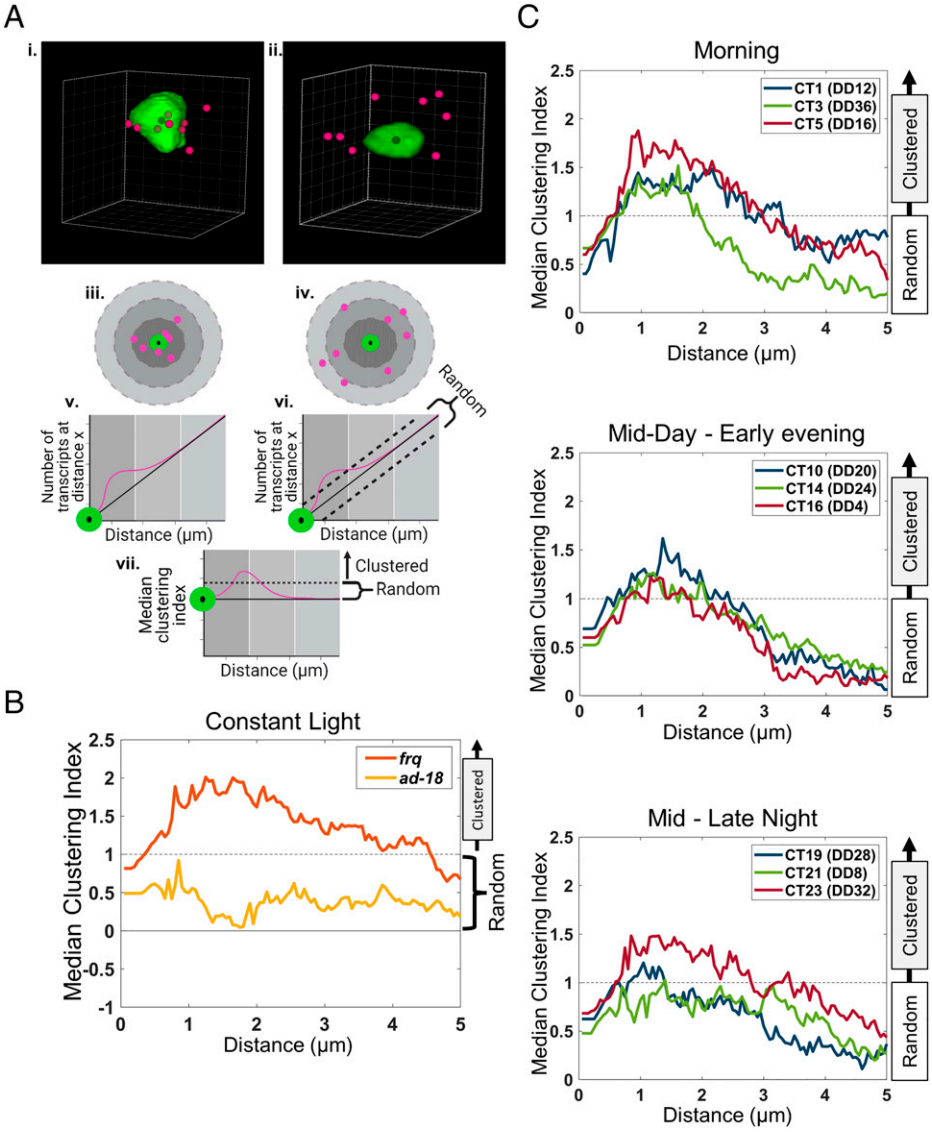

Fig. 3. *frequency* mRNA clusters with nuclei. (*A*) Spatial point patterning analysis using Ripley's K. Three-dimensional rendering of objects from real data detected by image analysis software. Transcripts (magenta) appear clustered near a nucleus (green) (*i*) or having no particular association (random) with a nucleus (*ii*). Black dots indicate the center of mass for the nuclei. The number of transcripts within spheres at increasing distances extending outward from the nuclear center of mass is quantified using Ripley's K function (*iii* and *iv*) and plotted (*v*). Nuclei with a high number of transcripts clustered within a sphere with radius *x* from the nuclear center of mass will show enrichment on the corresponding magenta line on the plot (*v*), whereas nuclei with transcripts randomly distributed from the nuclear center of mass will simply increase in a near-linear manner as shown with the black line on the plot (*v*). A 95% CI of random distribution is determined by a 100× simulation and represented by black dotted lines (*vi*). Data are normalized to the upper bounds of the 95% CI and a median clustering index is plotted in magenta (*vii*). Values where the curve is above the 95% CI random range indicate clustering with $P < 0.05$. (*B*) Clustering index of *frq* and *ad-18* in constant light. (*C*) Clustering index of *frq* throughout the day in free running (constant darkness) conditions.

transcripts per nucleus was 2.15, and the mean of *frq* transcripts per nucleus was 3.27. This less than twofold difference is consistent with the difference between *ad-18* and *frq* FPKM (Fragments Per Kilobase of transcript per Million mapped reads) values from previous RNA-sequencing analysis, which were 23 and 38, respectively (23). As expected, *ad-18* was not observed to be clustered relative to nuclei in constant light (Fig. 3*B*). Demonstrating that the observed clustering of *frq* transcripts does not reflect an aspect of light signaling, clusters of *frq* mRNA were similarly observed just outside nuclear boundaries at all times of day, with the exception of CT21, corresponding to the late subjective night, when *frq* expression is fully repressed. Clustering was strongest at times of peak circadian *frq* expression (CT23 to CT5, corresponding to late night through morning), and transcripts were found to be clustered with nuclei between 1 and 2.5 μm from the center of nuclei (Fig. 3*C*). Based on our observation that only about 30% of nuclei appear to be transcribing *frq* at its peak (DD16), we wondered what the relationship between transcript proximity to nuclei and transcription might be. To probe this, we measured the distance from the center of each nucleus to the nearest *frq* transcript at DD16 (*SI Appendix*, Fig. S1*C*). The mean value was 1.32 μm and 82% of nuclei had a transcript less than 2 μm from the center. With nuclear diameters ranging from 1 to 2 μm, this indicates that a significant percentage of nuclei have perinuclear *frq* transcripts, despite only a small subset actively producing it. We take this to suggest some form of active transport and distribution of *frq* mRNA. To better understand how this positioning might be facilitated, we turned to an mRNA-binding protein that preliminary data suggested might directly interact with *frq* and is known to affect period length.

The RNA-Binding Protein PRD-2 Influences *frq* Localization. The *prd-2* (*period-2*) gene in *Neurospora* was originally isolated nearly 40 y ago as a long-period mutant in an unbiased open

screen for period-length mutants (41). Despite the similarity in names, *Neurospora prd-2* bears no similarity to mammalian circadian repressor *Per2*, but instead PRD-2 has recently been shown to encode an RNA-binding protein that plays a critical role in protecting *ck-1a* (encoding casein kinase 1) transcripts from nonsense-mediated decay (23). Our unexpected observation of RNA localization suggested the obvious experiment of determining whether this RNA-binding protein influenced the RNA localization of *frq*. When a *Δprd-2* mutant strain was used for smFISH and Ripley's K analysis, we saw both in constant light and at CT5 that clustering of *frq* mRNAs with respect to nuclei was abolished (Fig. 4*A*). Controls indicated that the number of *frq* transcripts per nucleus was not different from wild type (compare Figs. 1*D* and 4*B*). The effect of PRD-2 on *frq* localization led to a natural interest in whether PRD-2 is directly interacting with *frq* mRNA or the effect is happening through some other mechanism. uvCLIP (RNA immunoprecipitation after ultraviolet cross-linking) analysis (23) of a strain expressing C-terminally FLAG-tagged PRD-2 from the native locus revealed significant albeit modest binding of *frq* by PRD-2 and binding of *ck-1a* that is consistent with previously reported data (Fig. 4*C*) (23). To estimate the relative specificity of the interaction between PRD-2 and mRNAs, and between *frq* transcript and mRNA-binding proteins, a different RNA-binding protein, PUF4, was used in the same protocol. The known interacting mRNA targets of PUF4, mRNAs encoded by *mrp-1* and *cbp3* (23, 42), were strongly bound by PUF4 but not by PRD-2, and *frq* mRNA was not bound by PUF4 (*SI Appendix*, Fig. S2*A*). In a parallel experiment to control for the epitope tag, PRD-2 tagged with mNeonGreen at its C terminus (PRD-2^{mNeonGreen}) was shown to bind *frq* mRNA to a degree similar to that seen for PRD-2^{FLAG} (*SI Appendix*, Fig. S2*B*). Actin was used to normalize all qPCR data. Although actin was thought to be a putative target of PUF4 (23, 42), analysis of enrichment of actin in PUF4 samples using an alternative normalizer, *crp43*, in our hands did not show significant enrichment (*SI Appendix*, Fig. S2*C*). These data suggest direct spatial regulation of *frq* mRNA by PRD-2, but do not explain a mechanism of trafficking. While a direct effect of PRD-2 on *frq* mRNA localization is the most straightforward interpretation of the data, PRD-2 also influences *ck-1a* levels, which in turn affect period length (23). Because of this, the possibility exists that the effect of PRD-2 on *frq* localization is due to increased phosphorylation by CK1 of an unknown substrate that in turn influences *frq* localization.

PRD-2 Is an Intrinsically Disordered Protein That Is Heterogeneously Localized in the Cytoplasm. To better understand the nature of the influence of PRD-2 on localization of *frq* transcripts, we used the PRD-2^{mNeonGreen} strain for live-cell imaging, with histone H1 (hH1) C-terminally tagged with mApple serving as a nuclear marker. PRD-2 was found heterogeneously localized in the cytoplasm and distinctly excluded from nuclei (Fig. 5*A* and Movie S1), consistent with the cytoplasmic localization of PRD-2 shown previously by subcellular fractionation (23). The live-cell imaging did, however, provide more detail in that PRD-2 was observed as discrete puncta that can be seen moving both in retrograde and anterograde on

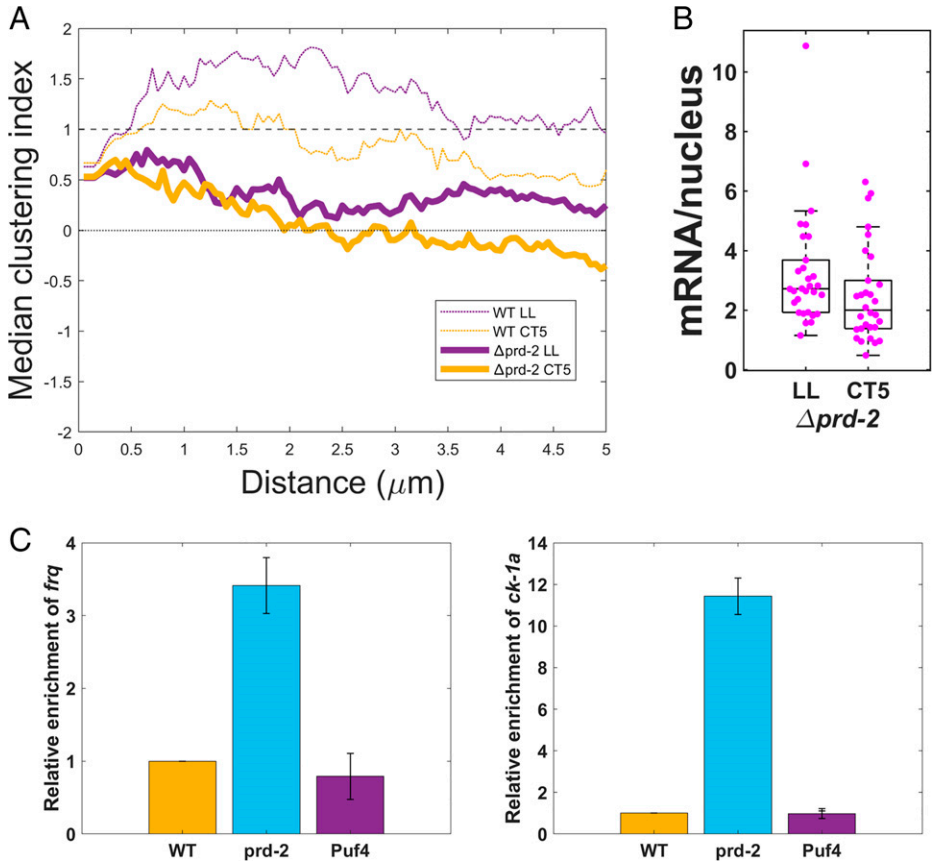

Fig. 4. RNA-binding protein PERIOD-2 influences *frq* localization. (*A*) Clustering index of *frq* in constant light (purple) and at CT5 (yellow) in a *Δprd-2* mutant strain, compared with wild type (thin dotted lines). (*B*) Boxplot of the ratio of *frq* mRNA to nuclei in *Δprd-2* hyphae in constant light and at CT5. Mean values are not statistically different from Fig. 1*D* wild type. (*C*) qRT-PCR performed on uvCLIP samples of PRD-2^{FLAG} and Puf4^{FLAG} using anti-FLAG–coated magnetic beads shows enrichment of *frq* and *ck-1a* in PRD-2 but not Puf4 samples (N = 3 biological replicates, error bars +/- SD). The mRNA produced by the actin gene was used for normalization.

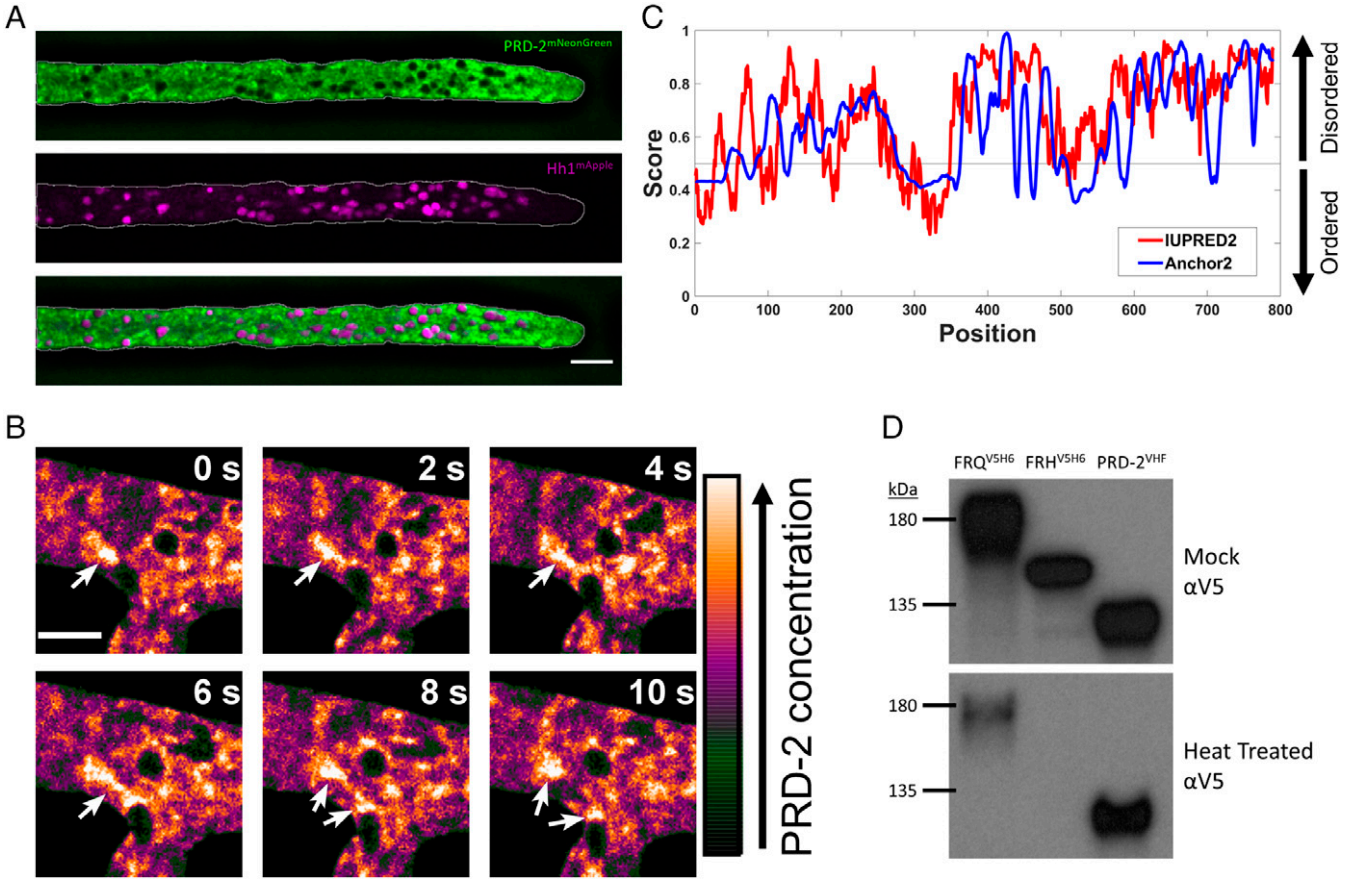

Fig. 5. PERIOD-2 is an intrinsically disordered cytoplasmic protein. (*A*) PRD-2 is heterogeneously localized in the cytoplasm as shown by PRD-2^{mNeonGreen} and histone H1^{mApple} in live cells. (Scale bar, 5 μm.) (*B*) Multicolored lookup table showing heterogeneous patterning of PRD-2^{mNeonGreen}. Approximately circular black regions within the cell are nuclei, from which PRD-2 is excluded. Arrows indicate a patch of enriched PRD-2 associating with a nucleus and being pulled apart into two distinct patches. (Scale bar, 4 μm.) (*C*) PRD-2 is predicted to be highly disordered by IUPred2 and ANCHOR2. Regions of the plot where a line exceeds a score of 0.5 are predicted to be part of a disordered region. (*D*) Intrinsically disordered proteins FRQ and PRD-2 remain in solution after incubating a lysate at 100 °C for 10 min, whereas the highly ordered protein FRH precipitates out.

different occasions at rates faster than bulk cytoplasmic flow, indicating interaction with motor proteins (Movies S2 and S3). PRD-2 is also seen as micrometer-scale patches that interact transiently with nuclei (Fig. 5*B* and Movies S1 and S4). A color gradient lookup table was employed to better visualize subtle differences in accumulation of PRD-2 throughout the hyphae. Elastic-like properties of PRD-2 can be seen by observing changes in large patches over time. Interaction with nuclei seems to pull large patches of PRD-2 apart and separate them in a manner similar to pulling a piece of caramel apart (Fig. 5*B* and Movie S4). These observations of the ability of PRD-2 to form dynamic and elastic higher-order structures led to an interest in its structure. Analysis of the polypeptide sequence of PRD-2 by the disorder-predicting algorithms IUPred2 and ANCHOR2 indicate that PRD-2 is very likely highly disordered with only a few structurally ordered domains (Fig. 5*C*) (43). To confirm the intrinsically disordered nature of PRD-2, we employed heat treatment which has been used previously to support the hypothesis that proteins, including circadian clock proteins FRQ and PER2, are disordered: Highly ordered proteins precipitate out of solution upon heat-driven denaturation whereas highly disordered proteins without much discernible structure remain in solution (15, 16). Lysates of strains containing V5 C-terminally tagged FRQ, FRH, and PRD-2 were heated at 100 °C for 10 min and centrifuged, and the resulting supernatants were analyzed by Western blot. While the highly structured FRH protein did not remain in solution, both PRD-2 and FRQ could still be readily observed (Fig. 5*D*). This finding supports the prediction that PRD-2 is an IDP.

One property of IDPs that has been established is their propensity to undergo liquid–liquid phase separation, which can take on many roles in cells (10). Of particular interest are reports that mRNA-interacting IDPs can play a role in mRNA sequestration and transport (44, 45). This phenomenon has been studied by fluorescently labeling IDPs and mRNA for visualization by light microscopy to observe the formation of spherical biomolecular condensates in vitro (45–48). To employ this method, PRD-2 was recombinantly expressed in *Escherichia coli*, purified by immobilized metal affinity chromatography, and tagged with Alexa Fluor 488 using NHS (*N*-hydroxysuccinimide)–ester chemistry (*SI Appendix*, Fig. S3*A*). *frq* mRNA was transcribed and tagged with Cy5 in vitro (*SI Appendix*, Fig. S3*B*). Through these experiments, PRD-2 has been observed forming spherical droplets in vitro (*SI Appendix*, Fig. S3*C*). However, in time, droplets stop growing in size and become more gel-like while retaining their spherical geometry. *frq* mRNA alone did not appear to form significant structures (*SI Appendix*, Fig. S3*D*). However, when combined, *frq* and PRD-2 form both droplets and large amorphous structures depending on salt and protein concentrations. Amorphous assemblies (formed in higher-salt conditions) have a central ring of colocalized mRNA and protein while spherical droplets (formed in lower-salt conditions) are less enriched for both components in the center (*SI Appendix*, Fig. S3 *E* and *F*). A central ring depleted of protein can also sometimes

be observed in the protein-only droplets (*SI Appendix*, Fig. S3 *C* and *E*). These data show that under physiological salt and protein conditions, PRD-2 and *frq* coassemble and PRD-2 has a propensity to form distinct higher-order structures, the nature of which is likely dictated by the local cytoplasmic environment, signaling, or potentially additional protein and RNA interactions found in the cell.

Discussion

Circadian oscillators are characterized by cycles in the expression of core component proteins and the mRNAs that encode them. Indeed, one of the universal molecular hallmarks of circadian oscillator mechanisms among animals and fungi is the hours-long delay between the peaks in clock-component mRNAs, their corresponding proteins, and the repressive complexes that they form. While recent years have seen significant growth in tools and insights contributing to our understanding of the spatiotemporal dynamics of core clock proteins in animals and fungi (6, 7, 27, 49–51), few studies have investigated the spatial dynamics and regulation of mRNA localization over circadian time that might contribute to such delays (52, 53). These significant delays, on the order of several hours between peak mRNA accumulation and peak protein accumulation in all systems, indicate a role for posttranscriptional regulation which could reasonably include trafficking and localization of mRNA molecules (22, 25, 54). The key findings presented here provide an enhanced depth of understanding to previously described phenomena, demonstrating a role for mRNA subcellular localization and trafficking in contributing to the regulation of the *Neurospora* molecular clock.

Analysis of *frq* mRNA over the circadian cycle using smFISH recapitulates the canonical rhythm that has been well-established in *Neurospora* using bulk assays (30) (Fig. 2), while revealing a previously unappreciated high level of spatial heterogeneity between different regions of hyphae. Molecular heterogeneity of biological processes throughout mycelia is a well-established phenomenon observed in many fungal systems (55–58) and this is now extended to nuclei coexisting in a single syncytial hypha. Our data suggest that the fraction of nuclei actively transcribing *frq* is generally low and oscillates between as few as 8% during the subjective night and as many as 32% in the subjective morning (Fig. 2*C*). How this heterogeneity of transcription activation of *frq* by the WCC is regulated is unclear and will be the subject of future live-cell imaging studies. We know that nuclei in some fungi including *Neurospora* undergo asynchronous division cycles, despite existing in a common cytoplasm (12, 59, 60). This indicates a partitioning of biomolecules in a shared cytoplasm and differential local nuclear environments. A major area of interest in fungal cell biology is how nuclei near one another cooperate or compete to divide labor (56). It is possible that this could simply be a matter of the ratio of FRQ to WCC favoring repression in varying parts of the cell. Another possibility could be a role for heterogeneity of chromatin remodeling, which has been shown to be important for the normal function of the clock (61–63). A spatiotemporal investigation of direct interaction between FRQ and the WCC inside nuclei using superresolution imaging or a sensitive fluorescence-based assay such as Förster resonance energy transfer could provide substantial insights into this phenomenon.

We observed a generally low abundance of *frq* transcripts, cycling between an average of 0.4 and 2.23 transcripts per nucleus in the subjective night and subjective morning, respectively (Fig. 2*D*). Interestingly, the mRNAs encoding a mammalian functional ortholog of *frq*, *Per2*, have been reported to show similar spatiotemporal dynamics, with *Per2* transcripts present at concentrations per nucleus nearly identical to what we have reported for *frq* (52). Although how such low concentrations of mRNAs can give rise to robust time-delayed protein rhythms remains a mystery, recent mathematical modeling of the *Neurospora* clock informed by preliminary data from this study suggests a mechanism: Robust circadian rhythms may be produced from limited mRNA expression in a syncytium wherein not all nuclei are producing *frq* and single digits of transcripts per nucleus are present (64). Specifically, this is possible when FRQ protein is freely diffusible and can enter every nucleus in a synchronous circadian rhythmic cycle, conditions consistent with preliminary data we have generated visualizing FRQ protein over the circadian cycle. Taken together, our data and the modeling of Zinn-Brooks and Roper (64) suggest the involvement of cytoplasmic partitioning and division of labor between nuclei in this syncytial system, a current area of interest in fungi that has been implicated in other processes in *Neurospora* (56, 65).

A unique observation arising from this work is the clustering of *frq* transcripts with nuclei at phases of high transcription, clustering that is later abolished when *frq* transcription falls (Fig. 3). FRQ protein has been reported to enter nuclei immediately after translation (66). Positioning of transcripts near nuclei, coupled with rapid import of the encoded protein, suggests a role for local translation of *frq*. We saw that the RNA-binding protein PRD-2 interacts directly with *frq* mRNA, and this clustering of *frq* near nuclei is abolished in its absence (Fig. 4). A similar mRNA–protein interaction is observed in *A. gossypii* in regulating another rhythmic process, the cell cycle. In this system, the RNA-binding protein Whi3 binds to the cyclin *CLN3* mRNA and positions it near nuclei (29). In addition to being RNA-binding proteins, a commonality between Whi3 and PRD-2 is their intrinsically disordered nature and ability to undergo liquid–liquid phase separation (45) (Fig. 5 and *SI Appendix*, Fig. S3). IDPs and liquid–liquid phase separation are implicated in a number of roles in mRNA trafficking and general cellular processes (10, 67) and liquid–liquid phase separation is likely temperature-dependent. Given this, it is tempting to speculate that the role of PRD-2 in influencing the formation of non–membrane-bound cellular compartments might in some way explain some of the more obscure general growth (e.g., noncircadian) characteristics of the original *prd-2[INV]* isolate (23, 41), for instance, the complete loss of temperature dependence of growth rate above 25 °C.

PRD-2 is observed in several different forms in the hyphae. We found discrete PRD-2 foci associating with cytoskeletal motor proteins (Movies S2 and S3) and large, dynamic, micrometer-scale patches associated with nuclei (Fig. 5*B* and Movies S1 and S4). While motor-associated PRD-2 foci were readily observed in many hyphae, this action may happen near tips more so than in central mycelial regions, where nuclear movement is often less dynamic. While PRD-2 can be seen throughout the cytoplasm as patches of different sizes (e.g., Fig. 5*A* and Movies S1, S2, S3, and S4), on average the slower-moving large patches that fuse with one another seem to be more prevalent. Future studies quantifying the spatial and temporal presence of the various forms observed for PRD-2's role in distributing RNAs throughout a mycelium may be revealing. From these data and our in vitro biochemical experiments showing the formation of PRD-2 condensates that incorporate *frq*, we can postulate a model in which *frq* mRNA is sequestered along with *ck-1a* mRNA by PRD-2 upon exiting nuclei, forming discrete condensates that can transport both transcripts along the cytoskeletal network, distributing it throughout the mycelium. The PRD-2–mediated clustering of *frq*

observed near nuclei is likely the result of accumulation of *frq* in PRD-2 condensates; fission and fusion of these condensates as suggested in Movies S1 and S4 could ensure that *frq* and *ck-1a*, which are spatially heterogeneously transcribed, are distributed throughout the mycelium to promote synchrony of the clock. In the absence of PRD-2 and this process, it is apparent that FRQ can still enter nuclei and carry out its repressive function. However, repression requires FRQ as well as CK1 in the repressive complex and, in the absence of PRD-2 clustering of these clock-relevant transcripts, the assembly of the FRQ–FRH–CK1 repressive complex and its nuclear accumulation might be slower, which could lead to the observed longer period. While this is plausible, attempts to define a unique clock phase for PRD-2 action have failed, likely due to the diverse effects of *prd-2* mutations. For instance, Lambreghts measured at 10-min intervals the activity of the WCC from trough to peak activity, as this is the part of the circadian cycle that encompasses the events surrounding FRQ translation and its return to the nucleus to shut off WCC activity and *frq* mRNA synthesis; he found no meaningful difference in the duration of this part of the cycle between wild type and *prd-2[mutant]* (68). More generally, loss of PRD-2 affects not only *frq* mRNA localization as we show here but also stability of *ck-1a* mRNA and therefore levels of CK1, which in turn affect period length by altering the stability of FRQ as well as slowing the inactivation of the WCC in the negative arm of the cycle. Thus, the effects of *prd-2* mutation are likely spread out over both the positive and negative arms of the cycle.

Foundational research in *Neurospora* has shown that in heterokaryons bearing nuclei having distinct *frq* alleles conferring different period-length clocks, the period length observed from the heterokaryotic mycelium is the weighted numerical average of the period lengths of the constituent alleles (69, 70). The phase separation data (Fig. 5, *SI Appendix*, Fig. S3, and Movies S1, S2, S3, and S4) we have presented may begin to explain this period averaging. Despite spatial heterogeneity in transcription, PRD-2–mediated distribution of *frq* mRNAs throughout the mycelium could lead to homogenization of different FRQ alleles within the cytoplasm as well as conferring clock regulation on nuclei not expressing *frq*. More generally, the involvement of PRD-2 in regulating *frq* localization gives us insights into the complexity of the *Neurospora* clock at the cellular level that has been previously unappreciated. Future studies employing live-cell mRNA and protein imaging techniques will allow us to further probe our hypotheses and improve our understanding of the cellular dynamics involved in the regulation of the *Neurospora* clock.

Materials and Methods

Strains Used. *N. crassa* 74-OR23-1VA (FGSC, 2489) was used as the wild-type strain in all smFISH experiments. FGSC11554 was produced as part of the *Neurospora crassa* knockout project (71) and was used as the Δ*frq* strain. To carry out smFISH in a Δ*prd-2* strain, the open reading frame (ORF) of NCU01019 (encoding *prd-2*) was replaced by the *bar* gene, conferring resistance to Bialaphos. Strains used in uvCLIP experiments, *prd-2*[V5-10XHis-3XFLAG] and *puf4*[V5-10XHis-3XFLAG], were generated for a previous study (23). IDP analysis was carried out using *frq*[V5-6XHis] and *frh*[V5-6XHis] (15), in addition to the previously mentioned *prd-2*[V5-10XHis-3XFLAG] strain. To construct the PRD-2^{mNeonGreen} strain, the rights to use mNeonGreen were purchased from Allele Biotechnology and an allele that was codon-optimized for *N. crassa* was synthesized by Integrated DNA Technologies. One thousand base pairs of DNA upstream of the PRD-2 stop codon, along with its 3′ untranslated region (UTR), and 1,000 bp downstream of the 3′ UTR were amplified from wild-type *N. crassa* DNA. The hygromycin B resistance–conferring DNA cassette was amplified from a plasmid obtained from the Fungal Genetics Stock Center. Overlapping primers were designed to insert the mNeonGreen peptide following an 8-bp linker at the 3′ end of the DNA fragment associated with the PRD-2 ORF, followed by the 3′ UTR, the hygromycin B resistance cassette, and finally the 1,000 bp of downstream genomic DNA homology. All DNA fragments and the vector (pRS426) were amplified by PCR using Q5 Hot Start High-Fidelity 2X Master Mix (New England Biolabs, M0494). The fragments were assembled using NEBuilder HIFI DNA Assembly Master Mix (New England Biolabs, E2621). NEB 5-alpha Competent *E. coli* (High Efficiency) (New England Biolabs, C2987) was used as the host for expansion of the assembled plasmid. The ∼5-kb transformation cassette was amplified by PCR and transformed into *N. crassa* conidia by electroporation using well-established protocols (71). Homokaryons were obtained by conducting a cross between the transformed heterokaryon and a homokaryon wild-type strain.

Single-Molecule RNA FISH. smFISH was adapted for use in *Neurospora* from a protocol for *A. gossypii* (28); the extensive adaptations made to the protocol are described in detail in a separate publication (27). Briefly, *N. crassa* conidiophores were used to inoculate 27 mL Vogel's liquid culture medium containing 2 g/L polyacrylic acid (72) in 125-mL Erlenmeyer flasks and were grown in constant light at 25 °C on an orbital shaker rotating at 100 rpm for 6 h. Growth in polyacrylic acid–containing medium inhibits the formation of large mycelial aggregates, yielding a highly dispersed culture (33). Cultures were transferred to the dark in an incubator maintaining 25 °C and continued shaking at 100 rpm until the circadian time point desired. Three milliliters of 37% formaldehyde stabilized with methanol was added to the cultures for fixation, which was carried out over 1 h with constant shaking at 100 rpm. Fixed cells were washed three times in ice-cold 1.2 M buffered sorbitol (pH 7.4). Enzymatic cell-wall digestion was carried out using 250 U/mL Zymolyase and 20 μg/mL recombinant chitinase under RNase-free conditions. After cell-wall removal, hyphae were washed three times with ice-cold 1.2 M buffered sorbitol (pH 7.4). Membrane permeabilization was carried out overnight in 70% EtOH at 4 °C. Permeabilized hyphae were washed three times at room temperature with wash buffer (2× saline sodium citrate, 10% deionized formamide). Custom mRNA probes conjugated with Quasar 670 or CAL Fluor Red 590 were hybridized to target cellular mRNAs overnight in Stellaris hybridization buffer (Biosearch Technologies, SMF-HB1-10) at 37 °C. Hyphae were washed three times with wash buffer at room temperature. During the second wash, 20 μM Hoechst 33342 was added to stain DNA for nuclear visualization and segmentation. Hyphae were mounted on glass slides with ProLong Glass Antifade Mountant (Invitrogen, P36984). Imaging was carried out using a Nikon Ti-E–based inverted microscope equipped with a Yokogawa CSU-W1 confocal scanner unit and Photometrics Prime BSI sCMOS cameras. We used a 60× oil immersion lambda series objective with a numerical aperture of 1.4. *Z* stacks were acquired and analyzed for all strains. Numerical data were extracted from imaging data and analyzed in the manner described by Lee and colleagues (28, 29) with the following exceptions. The Fiji macro written for *A. gossypii* produced a hyphal mask from phase-contrast images. This was inconsistent in our hands, and we therefore adapted it to create a mask from the fluorescent channels. *Neurospora* nuclei are closer in proximity to one another than in *Ashbya* and the nuclear segmenting methodology using the 3D Objects Counter plugin in Fiji was unreliable. We therefore created a custom nuclear segmentation pipeline using arivis Vision4D, which provided far superior differentiation of nuclei that were very close to each other. Three-dimensional nuclear and mRNA segmentation was used for colocalization analysis of mRNA inside nuclei using Vision4D. A threshold of 100% pixel overlap of a given mRNA punctum with its parent nucleus was used. We adapted the MATLAB code written for analysis of *Ashbya* by Lee and colleagues to read in segmentation data from Vision4D. Additional outputs were added to the MATLAB code to produce data tables of integrated density values for all mRNA foci and the ratio of mRNA to nuclei.

Statistical Analysis. All statistical analyses and graphical representations in this work were produced in MATLAB. The custom MATLAB code written by Lee and colleagues (28, 29) for spatial point patterning statistics was employed for the Ripley's K analysis of smFISH data. The mathematics implemented in this code are explained in great detail by Lee and colleagues. Briefly, the bivariate Ripley's K function [*K*(d)] (73) is used to determine the ratio of the average number of mRNA foci within a given radius from the center of each nucleus to the overall density of mRNA within the hyphal volume. A 100× randomization of

the number of mRNA foci is performed and $K_s(d)$ is calculated for each iteration to define a 95% CI of complete spatial randomness. The $H(d)$ function, which accounts for $K(d)$, given $K_s(d)$ is plotted and normalized to the upper bounds of the 95% CI. The median value from many analyzed cells is plotted as a median clustering index. At distances where the line breaches the 95% CI, this indicates statistically significant nonrandom clustering.

uvCLIP and qRT-PCR. uvCLIP for FLAG-tagged strains was carried out as described previously with the experimental and control strains used here (23). Briefly, *N. crassa* was grown from conidia in shaking liquid culture. The hyphae were collected on a Whatman qualitative filter disk (GE Healthcare Life Sciences, 1001-070) through a Buchner funnel attached to an aspiration trap to remove as much liquid as possible. Hyphal mats were immediately cross-linked by UV exposure in a Stratagene UV Stratalinker 1800 for 7 min on each side. The tissue was frozen in liquid nitrogen and ground into a powder with a mortar and pestle. RNase-free protein extraction was carried out by incubating about 300 μL hyphal powder with extraction buffer (25 mM Tris·HCl, pH 7.4, 150 mM NaCl, 2 mM $MgCl_2$, 0.5% Nonidet P-40, 1 mM dithiothreitol, 1× cOmplete protease inhibitor [Roche, 4693132001], and 100 U/mL RNaseOUT [Invitrogen, 10777019]) for 10 min at 4 °C on an end-over-end rotator and then on ice for another 5 min. After centrifugation to pellet cellular debris, supernatant containing 10 mg of total protein was incubated with 30 μL anti-FLAG beads (Millipore, M8823) for 4 h at 4 °C on an end-over-end rotator. Beads were washed three times with extraction buffer and ribonucleoprotein complexes were eluted from the beads with 100 μL 0.1 M glycine·HCl (pH 3.0). RNA was extracted from the eluate using the Direct-Zol RNA Microprep Kit (Zymo Research, R2060). The mNeonGreen-tagged strain was treated in the same manner to this point, with the exception that anti-mNeonGreen magnetic beads (ChromoTek, ntma) were used.

Purified RNA was prepared for qRT-PCR using the SuperScript IV First-Strand Synthesis System (Invitrogen, 18091050). qRT-PCR was carried out using iScript Reverse Transcription Supermix (Bio-Rad, 170-8841) on an Applied Biosystems StepOnePlus Real-Time PCR System. Data were analyzed using the ΔΔCt method with actin mRNA to normalize.

Live-Cell Imaging and Analysis. Live-cell imaging of prd-$2^{mNeonGreen}$ was carried out at room temperature on an Andor W-1 spinning disk confocal system on a Nikon Eclipse Ti-E inverted microscope stand. A 60× oil objective with a numerical aperture of 1.4 was used for imaging and an Andor Zyla 4.2 sCMOS camera was used to create digital images. A Piezo Z drive was used to acquire rapid *z* stacks. Images and movies for display were created with Fiji (74).

Additional methods can be found in *SI Appendix*.

Data Availability. All study data are included in the article and/or supporting information.

ACKNOWLEDGMENTS. We thank the Fungal Genetics Stock Center at Kansas State University for *Neurospora* strains, and Samantha Dundon, Christina Kelliher, and Wei Wang for advice and technical assistance. This work was supported by grants from the NIH to J.C.D. (R35GM118021) and J.J.L. (R35GM118022), Dartmouth's BioMT Core COBRE Grant P20-GM113132, and NIH Training Grant T32-008704 (to B.M.B.).

1. K. H. Cox, J. S. Takahashi, Circadian clock genes and the transcriptional architecture of the clock mechanism. *J. Mol. Endocrinol.* **63**, R93–R102 (2019).
2. A. Taton *et al.*, The circadian clock and darkness control natural competence in cyanobacteria. *Nat. Commun.* **11**, 1688 (2020).
3. M. Greenwood, J. C. Locke, The circadian clock coordinates plant development through specificity at the tissue and cellular level. *Curr. Opin. Plant Biol.* **53**, 65–72 (2020).
4. J. J. Loros, Principles of the animal molecular clock learned from *Neurospora*. *Eur. J. Neurosci.* **51**, 19–33 (2020).
5. Y. Liu, D. Bell-Pedersen, Circadian rhythms in *Neurospora crassa* and other filamentous fungi. *Eukaryot. Cell* **5**, 1184–1193 (2006).
6. N. J. Smyllie *et al.*, Visualizing and quantifying intracellular behavior and abundance of the core circadian clock protein PERIOD2. *Curr. Biol.* **26**, 1880–1886 (2016).
7. Y. Xiao, Y. Yuan, M. Jimenez, N. Soni, S. Yadlapalli, Clock proteins regulate spatiotemporal organization of clock genes to control circadian rhythms. *Proc. Natl. Acad. Sci. U.S.A.* **118**, e2019756118 (2021).
8. P. Meyer, L. Saez, M. W. Young, PER-TIM interactions in living *Drosophila* cells: An interval timer for the circadian clock. *Science* **311**, 226–229 (2006).
9. C. Luo, J. J. Loros, J. C. Dunlap, Nuclear localization is required for function of the essential clock protein FRQ. *EMBO J.* **17**, 1228–1235 (1998).
10. S. F. Banani, H. O. Lee, A. A. Hyman, M. K. Rosen, Biomolecular condensates: Organizers of cellular biochemistry. *Nat. Rev. Mol. Cell Biol.* **18**, 285–298 (2017).
11. G. A. McLaughlin *et al.*, Spatial heterogeneity of the cytosol revealed by machine learning-based 3D particle tracking. *Mol. Biol. Cell* **31**, 1498–1511 (2020).
12. S. E. Roberts, A. S. Gladfelter, Nuclear autonomy in multinucleate fungi. *Curr. Opin. Microbiol.* **28**, 60–65 (2015).
13. J. C. Dunlap, Molecular bases for circadian clocks. *Cell* **96**, 271–290 (1999).
14. A. Patke, M. W. Young, S. Axelrod, Molecular mechanisms and physiological importance of circadian rhythms. *Nat. Rev. Mol. Cell Biol.* **21**, 67–84 (2020).
15. J. M. Hurley, L. F. Larrondo, J. J. Loros, J. C. Dunlap, Conserved RNA helicase FRH acts nonenzymatically to support the intrinsically disordered *Neurospora* clock protein FRQ. *Mol. Cell* **52**, 832–843 (2013).
16. J. F. Pelham, J. C. Dunlap, J. M. Hurley, Intrinsic disorder is an essential characteristic of components in the conserved circadian circuit. *Cell Commun. Signal.* **18**, 181 (2020).
17. C. L. Baker, A. N. Kettenbach, J. J. Loros, S. A. Gerber, J. C. Dunlap, Quantitative proteomics reveals a dynamic interactome and phase-specific phosphorylation in the *Neurospora* circadian clock. *Mol. Cell* **34**, 354–363 (2009).
18. C.-T. Tang *et al.*, Setting the pace of the *Neurospora* circadian clock by multiple independent FRQ phosphorylation events. *Proc. Natl. Acad. Sci. U.S.A.* **106**, 10722–10727 (2009).
19. B. Wang, A. N. Kettenbach, X. Zhou, J. J. Loros, J. C. Dunlap, The phospho-code determining circadian feedback loop closure and output in *Neurospora*. *Mol. Cell* **74**, 771–784.e3 (2019).
20. L. F. Larrondo, C. Olivares-Yañez, C. L. Baker, J. J. Loros, J. C. Dunlap, Circadian rhythms. Decoupling circadian clock protein turnover from circadian period determination. *Science* **347**, 1257277 (2015).
21. N. Y. Garceau, Y. Liu, J. J. Loros, J. C. Dunlap, Alternative initiation of translation and time-specific phosphorylation yield multiple forms of the essential clock protein FREQUENCY. *Cell* **89**, 469–476 (1997).
22. J. M. Hurley *et al.*, Analysis of clock-regulated genes in *Neurospora* reveals widespread posttranscriptional control of metabolic potential. *Proc. Natl. Acad. Sci. U.S.A.* **111**, 16995–17002 (2014).
23. C. M. Kelliher *et al.*, PRD-2 directly regulates *casein kinase I* and counteracts nonsense-mediated decay in the *Neurospora* circadian clock. *eLife* **9**, e64007 (2020).
24. L. Lauinger *et al.*, Thiolutin is a zinc chelator that inhibits the Rpn11 and other JAMM metalloproteases. *Nat. Chem. Biol.* **13**, 709–714 (2017).
25. J. M. Hurley *et al.*, Circadian proteomic analysis uncovers mechanisms of post-transcriptional regulation in metabolic pathways. *Cell Syst.* **7**, 613–626.e5 (2018).
26. C. Lee, J.-P. Etchegaray, F. R. Cagampang, A. S. Loudon, S. M. Reppert, Posttranslational mechanisms regulate the mammalian circadian clock. *Cell* **107**, 855–867 (2001).
27. B. M. Bartholomai, A. S. Gladfelter, J. J. Loros, J. C. Dunlap, Quantitative single molecule RNA-FISH and RNase-free cell wall digestion in *Neurospora crassa*. *Fungal Genet. Biol.* **156**, 103615 (2021).
28. C. Lee, S. E. Roberts, A. S. Gladfelter, Quantitative spatial analysis of transcripts in multinucleate cells using single-molecule FISH. *Methods* **98**, 124–133 (2016).
29. C. Lee *et al.*, Protein aggregation behavior regulates cyclin transcript localization and cell-cycle control. *Dev. Cell* **25**, 572–584 (2013).
30. B. D. Aronson, K. A. Johnson, J. J. Loros, J. C. Dunlap, Negative feedback defining a circadian clock: Autoregulation of the clock gene frequency. *Science* **263**, 1578–1584 (1994).
31. S. K. Crosthwaite, J. J. Loros, J. C. Dunlap, Light-induced resetting of a circadian clock is mediated by a rapid increase in frequency transcript. *Cell* **81**, 1003–1012 (1995).
32. V. D. Gooch *et al.*, Fully codon-optimized luciferase uncovers novel temperature characteristics of the *Neurospora* clock. *Eukaryot. Cell* **7**, 28–37 (2008).
33. C. M. Kelliher, J. J. Loros, J. C. Dunlap, Evaluating the circadian rhythm and response to glucose addition in dispersed growth cultures of *Neurospora crassa*. *Fungal Biol.* **124**, 398–406 (2020).
34. T. L. Lenstra, J. Rodriguez, H. Chen, D. R. Larson, Transcription dynamics in living cells. *Annu. Rev. Biophys.* **45**, 25–47 (2016).
35. T. Chen, B. van Steensel, Comprehensive analysis of nucleocytoplasmic dynamics of mRNA in *Drosophila* cells. *PLoS Genet.* **13**, e1006929 (2017).
36. Y. Li, S. L. Junod, A. Ruba, J. M. Kelich, W. Yang, Nuclear export of mRNA molecules studied by SPEED microscopy. *Methods* **153**, 46–62 (2019).
37. A. Mor *et al.*, Dynamics of single mRNP nucleocytoplasmic transport and export through the nuclear pore in living cells. *Nat. Cell Biol.* **12**, 543–552 (2010).
38. B. D. Ripley, The second-order analysis of stationary point processes. *J. Appl. Probab.* **13**, 255–266 (1976).
39. P. M. Dixon, "Ripley's K function" in *Encyclopedia of Environmetrics*, A. H. El-Shaarawi, W. W. Piegorsch, Eds. (2001), (John Wiley & Sons) vol. 3, p. 1796.
40. A. J. Shatkin, E. L. Tatum, Electron microscopy of *Neurospora crassa* mycelia. *J. Biophys. Biochem. Cytol.* **6**, 423–426 (1959).
41. G. F. Gardner, J. F. Feldman, Temperature compensation of circadian period length in clock mutants of *Neurospora crassa*. *Plant Physiol.* **68**, 1244–1248 (1981).
42. D. Wilinski *et al.*, Recurrent rewiring and emergence of RNA regulatory networks. *Proc. Natl. Acad. Sci. U.S.A.* **114**, E2816–E2825 (2017).
43. G. Erdős, Z. Dosztányi, Analyzing protein disorder with IUPred2A. *Curr. Protoc. Bioinformatics* **70**, e99 (2020).
44. C. Roden, A. S. Gladfelter, RNA contributions to the form and function of biomolecular condensates. *Nat. Rev. Mol. Cell Biol.* **22**, 183–195 (2021).
45. H. Zhang *et al.*, RNA controls polyQ protein phase transitions. *Mol. Cell* **60**, 220–230 (2015).
46. S. Alberti, A. Gladfelter, T. Mittag, Considerations and challenges in studying liquid-liquid phase separation and biomolecular condensates. *Cell* **176**, 419–434 (2019).
47. E. M. Langdon *et al.*, mRNA structure determines specificity of a polyQ-driven phase separation. *Science* **360**, 922–927 (2018).
48. E. M. Langdon, A. S. Gladfelter, Probing RNA structure in liquid-liquid phase separation using SHAPE-MaP. *Methods Enzymol.* **611**, 67–79 (2018).
49. C. H. Gabriel *et al.*, Live-cell imaging of circadian clock protein dynamics in CRISPR-generated knock-in cells. *Nat. Commun.* **12**, 3796 (2021).
50. N. Yang *et al.*, Quantitative live imaging of Venus:BMAL1 in a mouse model reveals complex dynamics of the master circadian clock regulator. *PLoS Genet.* **16**, e1008729 (2020).
51. V. Sabado, E. Nagoshi, "Fluorescence live imaging of *Drosophila* circadian pacemaker neurons" in *Circadian Clocks*, S. A. Brown, Ed. (Springer, 2021), pp. 207–219.

52. S. Wen *et al.*, Spatiotemporal single-cell analysis of gene expression in the mouse suprachiasmatic nucleus. *Nat. Neurosci.* **23**, 456–467 (2020).
53. N. E. Phillips *et al.*, The circadian oscillator analysed at the single-transcript level. *Mol. Syst. Biol.* **17**, e10135 (2021).
54. A. Nakashima *et al.*, DEC1 modulates the circadian phase of clock gene expression. *Mol. Cell. Biol.* **28**, 4080–4092 (2008).
55. C. de Bekker, O. Bruning, M. J. Jonker, T. M. Breit, H. A. Wösten, Single cell transcriptomics of neighboring hyphae of *Aspergillus niger*. *Genome Biol.* **12**, R71 (2011).
56. A. P. Mela, A. M. Rico-Ramírez, N. L. Glass, Syncytia in fungi. *Cells* **9**, 2255 (2020).
57. H. A. Wösten, G. J. van Veluw, C. de Bekker, P. Krijgsheld, Heterogeneity in the mycelium: Implications for the use of fungi as cell factories. *Biotechnol. Lett.* **35**, 1155–1164 (2013).
58. B. Zacchetti, H. A. B. Wösten, D. Claessen, Multiscale heterogeneity in filamentous microbes. *Biotechnol. Adv.* **36**, 2138–2149 (2018).
59. A. S. Gladfelter, A. K. Hungerbuehler, P. Philippsen, Asynchronous nuclear division cycles in multinucleated cells. *J. Cell Biol.* **172**, 347–362 (2006).
60. M. G. Roca, H.-C. Kuo, A. Lichius, M. Freitag, N. D. Read, Nuclear dynamics, mitosis, and the cytoskeleton during the early stages of colony initiation in *Neurospora crassa*. *Eukaryot. Cell* **9**, 1171–1183 (2010).
61. W. J. Belden, J. J. Loros, J. C. Dunlap, Execution of the circadian negative feedback loop in *Neurospora* requires the ATP-dependent chromatin-remodeling enzyme CLOCKSWITCH. *Mol. Cell* **25**, 587–600 (2007).
62. W. J. Belden, Z. A. Lewis, E. U. Selker, J. J. Loros, J. C. Dunlap, CHD1 remodels chromatin and influences transient DNA methylation at the clock gene frequency. *PLoS Genet.* **7**, e1002166 (2011).
63. Q. Zhu, W. J. Belden, Molecular regulation of circadian chromatin. *J. Mol. Biol.* **432**, 3466–3482 (2020).
64. L. Zinn-Brooks, M. L. Roper, Circadian rhythm shows potential for mRNA efficiency and self-organized division of labor in multinucleate cells. *PLoS Comput. Biol.* **17**, e1008828 (2021).
65. L. Pieuchot *et al.*, Cellular subcompartments through cytoplasmic streaming. *Dev. Cell* **34**, 410–420 (2015).
66. A. C. Diernfellner, C. Querfurth, C. Salazar, T. Höfer, M. Brunner, Phosphorylation modulates rapid nucleocytoplasmic shuttling and cytoplasmic accumulation of *Neurospora* clock protein FRQ on a circadian time scale. *Genes Dev.* **23**, 2192–2200 (2009).
67. E. M. Langdon, A. S. Gladfelter, A new lens for RNA localization: Liquid-liquid phase separation. *Annu. Rev. Microbiol.* **72**, 255–271 (2018).
68. R. Lambreghts, "Exploring new players in the *Neurospora* core clock and its output," doctoral dissertation, Dartmouth College, Hanover, NH (2012).
69. J. F. Feldman, M. N. Hoyle, Complementation analysis of linked circadian clock mutants of *Neurospora crassa*. *Genetics* **82**, 9–17 (1976).
70. J. J. Loros, A. Richman, J. F. Feldman, A recessive circadian clock mutation at the frq locus of *Neurospora crassa*. *Genetics* **114**, 1095–1110 (1986).
71. P. D. Collopy *et al.*, "High-throughput construction of gene deletion cassettes for generation of *Neurospora crassa* knockout strains" in *Molecular and Cell Biology Methods for Fungi*, A. Sharon, Ed. (Springer, 2010), pp. 33–40.
72. H. J. Vogel, A convenient growth medium for *Neurospora* (medium N). *Microb. Genet. Bull.* **13**, 42–43 (1956).
73. B. D. Ripley, *Spatial Statistics* (Wiley Series in Probability and Mathematical Statistics: Applied Probability & Mathematical Section, John Wiley & Sons, 1981).
74. J. Schindelin *et al.*, Fiji: An open-source platform for biological-image analysis. *Nat. Methods* **9**, 676–682 (2012).